Fission Fragment Anisotropy and Pairing Effects on Nuclear Structure*

R. Vandenbosch, H. Warhanek,† and J. R. Huizenga
Argonne National Laboratory, Argonne, Illinois
(Received June 26, 1961)

The dependence of the angular distributions on projectile energy for helium-ion-induced fission of Th^{232}, U^{233}, and U^{238} has been investigated using solid-state fission fragment detectors. The measurements cover the range of projectile energies between 20 and 43 Mev in steps of 1 Mev or less. The energy dependence of the anisotropy has a structure which is in qualitative agreement with theoretical predictions. The most fissionable target studied, U^{233}, shows the least structure while the least fissionable target, Th^{232}, shows the most structure, demonstrating that large anisotropies result from fission occurring at low excitation energy following neutron emission from the compound nucleus. The energy dependence of K_0, the standard deviation of the distribution in the angular-momentum projection on the nuclear symmetry axis at the saddlepoint, has been deduced from these and other data on angular distributions from neutron-induced fission. At high excitation energies K_0 is consistent with predictions of statistical theory with a moment of inertia close to that of a rigid rotator. At excitation energies in excess of the fission threshold of 10 Mev or less, K_0 is much reduced due to nuclear pairing effects.

I. INTRODUCTION

MANY experiments relating to fission fragment angular distributions have been performed during the last decade, and references to most of these works can be found in recent review papers.[1,2] The quantitative interpretation of these experiments has arisen from various applications of a general model proposed by Bohr.[3] The first successes of this model were in the interpretation of angular distributions for fission near threshold.[3,4] The model has since been extended by Strutinskii,[5] Halpern and Strutinskii,[6] and Griffin[7] to higher excitations, where many nuclear states are present and statistical considerations can be used. It is interesting to note that the recent interest in fission fragment angular distributions centers not on the fission process itself but rather on the information it provides on nuclear structure, particularly the pairing interaction.[8]

The present experiments were undertaken to investigate in some detail the energy dependence of fission fragment anisotropies. Although investigations of neutron-induced fission have given a fairly complete picture for low excitation energies, experiments at higher energies have not been extensive enough to

enable one to draw quantitative conclusions. Since a previous investigation[6,9] suggested a phase transition at excitation energies in excess of the fission threshold of between 10 and 15 Mev it was felt that a careful study of the energy dependence of helium-ion-induced fission would provide a more quantitative determination of this effect.

II. EXPERIMENTAL

A. Energy Degrading System and Scattering Chamber

In order to measure accurately the energy dependence of the anisotropy it was necessary to have a beam of particles whose energy could be varied in small steps over a wide range of energies. As the Argonne cyclotron is a fixed frequency accelerator, it is not possible to vary the energy of the emergent particles. It is therefore necessary to vary the energy by foil degradation, for which purpose an efficient energy degrading-focusing system has recently been developed[10] by the cyclotron group. As used in the present experiments the emergent beam is focused, deflected through 30°, and degraded and refocused. The degraded beam passes through a wall to the experimental tunnel where the scattering chamber is located. Focusing and deflection coils in the tunnel assure control of the beam. The degrading unit consists of remotely controlled water-cooled foils which are used not only to degrade the beam but also to determine the energy of the beam by range measurements. Mean ranges were converted to particle energies using range-energy curves constructed from the proton range-energy measurements of Bichsel,[11,12] assuming that the energy loss $-dE/dX$ has the same velocity dependence $F(v)$ for different particles so that $R = M/Z^2 F(v)$.

The scattering chamber is 11 in. in diameter, and is

* Based on work performed under the auspices of the U. S. Atomic Energy Commission.
† Permanent address: Institut für Radiumforschung, Vienna, Austria.
[1] I. Halpern, Ann. Rev. Nuclear Sci. **9**, (1959).
[2] J. R. Huizenga and R. Vandenbosch, *Nuclear Reactions*, edited by P. M. Endt and M. Demeur [North-Holland Publishing Company, Amsterdam (to be published)], Vol. II.
[3] A. Bohr, *Proceedings of the International Conference on the Peaceful Uses of Atomic Energy, Geneva, 1955* (United Nations, New York, 1956), Vol. 2, p. 151.
[4] L. Wilets and D. M. Chase, Phys. Rev. **103**, 1296 (1956).
[5] V. M. Strutinskii, Atomnaya Energ. **2**, 508 (1957) [translation: Soviet J. Atomic Energy **2**, 621 (1957)].
[6] I. Halpern and V. M. Strutinskii, *Proceedings of the Second United Nations International Conference on the Peaceful Uses of Atomic Energy, Geneva, 1958* (United Nations, Geneva, 1958), Vol. 15, p. 408.
[7] J. J. Griffin, Phys. Rev. **116**, 107 (1959).
[8] J. J. Griffin, *Proceedings of the International Conference on Nuclear Structure, Kingston, Canada, 1960* (University of Toronto Press, Toronto, 1960), p. 843.

[9] C. T. Coffin and I. Halpern, Phys. Rev. **112**, 536 (1958).
[10] W. J. Ramler, J. L. Yntema, and M. Oselka, Nuclear Instr. and Methods **8**, 217 (1960).
[11] H. Bichsel, Phys. Rev. **112**, 1089 (1958).
[12] H. Bichsel, R. F. Mozley, and W. A. Aron, Phys. Rev. **105**, 1788 (1957).

equipped with two movable detector holders which can be rotated independently. In the present experiment the detectors were located 4 in. from the target, which can also be rotated. With the detectors and geometry used the angular resolution was 3°. The collimating system used restricted the image of the beam at the target to a diameter of $\frac{1}{8}$ in.

B. Target Preparation

The targets were prepared by electrodeposition of 100–200 μg per square centimeter of the fissionable material onto 1-mil aluminum backing foils. The U^{233} target had an isotopic composition of 98.3% U^{233}, 0.13% U^{234}, 0.01% U^{235}, and 1.53% U^{238}. The U^{238} target was 99.9% isotopically pure. The Th^{232} is monoisotopic.

C. Fission Fragment Detectors

The solid-state detectors used in this study were prepared by D. M. Sparlin at this laboratory. They were made by evaporation of metallic gold onto silicon wafers. The sensitive area of the detectors was approximately 6 mm in diameter. The important advantage of the solid-state detectors is that these detectors can be constructed with an almost negligible window thickness, while the depth of the sensitive region of the detector can be adjusted by the magnitude of the reverse bias potential to correspond to the range of the fission fragments. Thus more energetic particles with longer ranges, such as scattered alpha particles, deposit only a small fraction of their energy in the sensitive region of the detector. This leads to a larger separation of the pulse heights for the fission fragments from the undesirable background from other particles. The detectors were usually operated at a reverse bias of 3–6 v.

D. Electronics

A schematic diagram of the electronic system used in these experiments is shown in Fig. 1. The preamps were attached directly to the scattering chamber, and had a gain of approximately 50. The signals from the preamps were fed by cables approximately 150 ft to the counting area. The pulses were amplified and then fed into single-channel analyzers that were used as integral discriminators. Their discrimination levels were adjusted so as to discriminate against most of the pile-up pulses caused by scattered alpha particles. Using their output pulses as gating pulses it was then possible to prevent the 256-channel analyzer from sorting these pulses, thus reducing the deadtime of the analyzer. Through use of scalers the single-channel analyzers also allowed a quick check on the counting rates of the two detectors. The signals from the two amplifiers were fed into alternate halves of the 256-channel analyzer, utilizing a routing pulse from a discriminator circuit in one of the amplifiers. Thus it was possible to record spectra from the two detectors simultaneously, eliminating errors due to
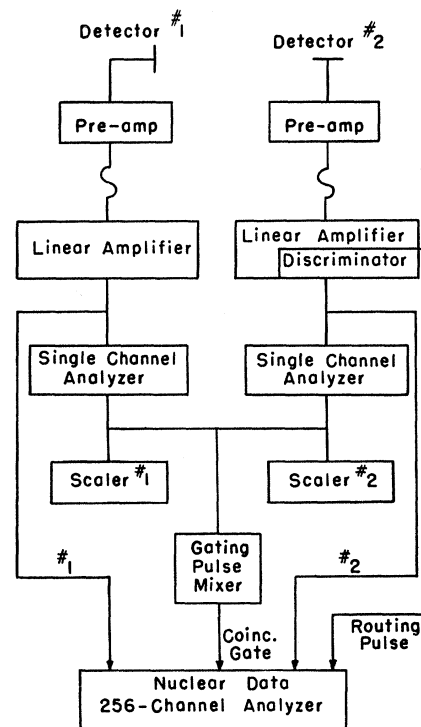

FIG. 1. Schematic diagram of the electronic system used with the solid-state detectors.

beam current integration, etc. Using the 256-channel analyzer in this way it is dead for receiving any pulse when sorting out a pulse in either of the two halves. In other words it has a common dead time for the two halves. The fission fragment pulses were well resolved from the scattered alpha-particle pile-up pulses. A correction was made for the small percentage ($<3\%$) of fission pulses which were in the overlap region between the pile-up and fission peaks.

III. RESULTS

A. Angular Distributions

Measurements of the details of the angular distribution were made at two energies for each of the targets studied. In these measurements one of the detectors was fixed at 190° (170°) with respect to the beam direction while the other detector was placed at different angles between 85° and 176°. At each angle for the movable detector the target was placed at an angle such that the angle between the detector and a line perpendicular to the target plane was equal for the two detectors. This meant that the average target thickness traversed by fission fragments was the same for either detector. This procedure was actually unnecessary, as it was shown that there was no difference in counting ratios for the case where the target plane was perpendicular to the detector compared with the case for the target plane at 40° with respect to the detector. The counting times were long enough such that the statistical uncertainty

was less than 1%. The laboratory angular distributions were converted to center-of-mass coordinates assuming full momentum transfer of the incident helium ion to the compound nucleus,[13] and also assuming all fission fragments had the same kinetic energy. The kinetic energy release for the different targets was estimated from the compilation of Halpern.[1] The center-of-mass angular distributions obtained are illustrated in Fig. 2. The angular distributions were analyzed in terms of Legendre polynomials by a least-squares procedure. The expansion coefficients obtained are given in Table I, and the resulting distributions are shown as the solid

TABLE I. Expansion coefficients for least-squares Legendre polynomial fit to the angular distributions. $W(\theta)=1+\alpha_2 P_2(\cos\theta) +\alpha_4 P_4(\cos\theta)+\alpha_6 P_6(\cos\theta)$.

	α_2	α_4	α_6
Th^{232}			
42 Mev	0.379±0.003	0.107±0.004	0.028±0.004
29.9 Mev	0.312±0.004	0.081±0.006	0.015±0.006
U^{238}			
43 Mev	0.286±0.004	0.074±0.005	0.002±0.006
37 Mev	0.230±0.009	0.056±0.011	−0.007±0.011
U^{233}			
41.7 Mev	0.248±0.003	0.030±0.004	0.006±0.004
32.3 Mev	0.202±0.005	0.013±0.007	−0.003±0.007

lines in Fig. 2. Expansions with terms of higher order than P_6 were tried but the coefficients of the higher terms were small and not statistically significant. Thus there is no direct evidence from this type of analysis that there is greater than 3 units of orbital angular momentum between the fragments, whereas the average angular momentum brought in by 43-Mev alpha particles is $12\hbar$. The neutrons may carry off some of this angular momentum, but recent experiments on isomer ratios for shielded fission fragments show that much of it shows up as spin of the final fragments.[14]

B. Energy Dependence of Anisotropy

In these experiments the two detectors were placed at 90° and 174° with respect to the beam direction. The corresponding center-of-mass angles are only slightly dependent on the bombarding energy, being approximately 92° and 174.3°, respectively. The anisotropy was measured for the three targets at energy intervals of 1 Mev or less. Periodic range measurements of the cyclotron beam were made to check the energy of the beam. The measured anisotropies, corrected to the center-of-mass system, are illustrated in Fig. 3. The anisotropies for Th^{232} and U^{238} at 43 Mev are in good agreement with the data of Coffin and Halpern[9] obtained by the catcher foil technique.

IV. COMPARISON WITH THEORY

A. Qualitative Considerations

From previous work on fission fragment angular distributions, both experimental and theoretical, it is possible to explain qualitatively our observed results. Fission fragment anisotropy increases with increasing angular momentum of the compound nucleus (associated with increasing bombarding energy) and increases with decreasing excitation energy (associated with decreasing bombarding energy or with fission following deexcitation by neutron emission). Thus for the same bombarding energy (same angular momentum for the compound nuclei) Th^{232} has a larger anisotropy than U^{233} because the system formed by bombarding Th^{232}
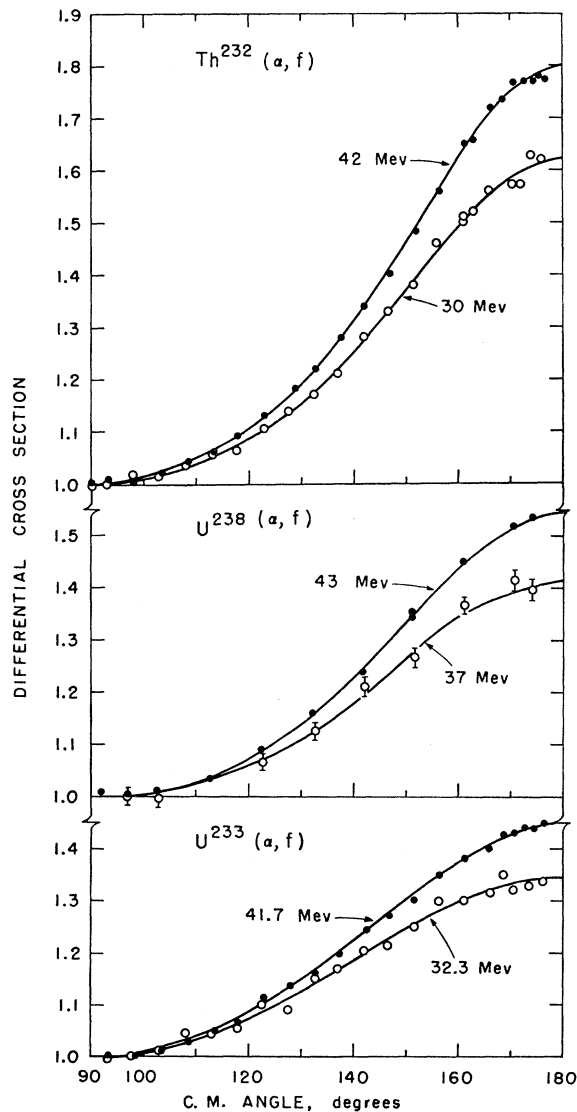

FIG. 2. Center-of-mass angular distributions at two energies for each of the targets studied. The standard deviations are approximately the size of the symbols except for U^{238} where the errors are somewhat larger. The solid lines represent least-squares fits to a Legendre polynomial expansion. The expansion coefficients are given in Table I.

[13] W. J. Nicholson and I. Halpern, Phys. Rev. 116, 175 (1959).

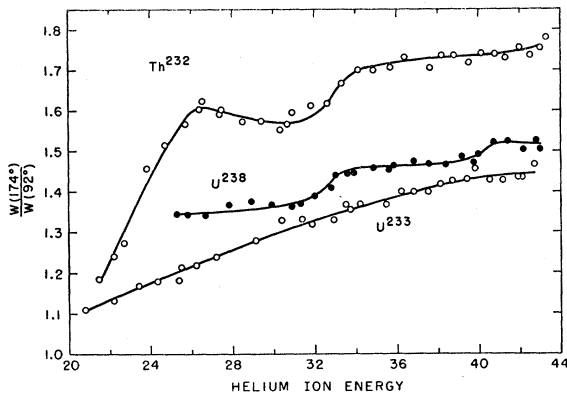[14] H. Warhanek and R. Vandenbosch (unpublished data).

FIG. 3. Energy dependence of the fission fragment anisotropies for the three targets studied. The ordinate is the ratio of the differential cross section at 174° (center of mass) to the differential cross section at approximately 92° (center of mass). The standard deviations are approximately the size of the symbols. The solid lines are smooth curves through the experimental data.

has a greater probability for emitting neutrons prior to fission than does the more fissionable system formed by bombarding U^{233}. This can be seen from the fractional fissionabilities[15] illustrated in Fig. 4. Of 100 U^{236} compound nuclei, only 35% fission prior to neutron emission, whereas 83% of the Pu^{237} compound nuclei fission prior to neutron emission. The larger the fraction of fission following neutron emission the lower is the average excitation energy at which fission occurs, resulting in a larger anisotropy as illustrated in Fig. 3. The structure observed is then associated with the onset of each new (α,xnf) process. The spacing between the jumps is of the order of the energy carried away by a neutron, binding plus average kinetic energy, which is approximately 6–8 Mev. The structure is not observed in the bombardment of U^{233} because so few nuclei survive first-chance fission to fission following neutron emission.

B. Quantitative Calculations

The theoretical framework for treating fission fragment angular distributions was proposed by Bohr.[3] Neglecting the spin of the target nucleus, the differential cross section at angle θ with respect to the beam direction is given by

$$W(\theta) \propto \int dI \int dK \, F(K,I)[\sin^2\theta - (K^2/I^2)]^{-\frac{1}{2}}, \quad (1)$$

where I is the total angular momentum, and K is the projection of I on the nuclear symmetry axis. The function $F(K,I)$ gives the distribution in K and I of the fissioning nucleus at the saddle point, and is assumed to be equal to a product of the factors $f(I)$ and $g(K)$. The theory has been developed in more detail for excita-

tion energies where sufficient states are available to use statistical considerations by Strutinskii,[5] Halpern and Strutinskii,[6] and Griffin.[7] The developments are rather similar, differing primarily in that Halpern and Strutinskii assume a Gaussian form for the distribution in K whereas Griffin[7] uses a linear form. We have somewhat arbitrarily chosen to use the Gaussian form for $g(K)$, partly because a larger body of low-energy neutron-induced angular distributions[16] has been analyzed in this framework and partly because it has been suggested[17] that the low-energy anisotropy of targets with different spins is better accounted for with a Gaussian K distribution. Taking $g(K) \propto \exp(-K^2/2K_0^2)$, Halpern and Strutinskii[6] have integrated Eq. (1) over K to give

$$W(\theta) \propto \int dI \, F(I)I/2K_0$$

$$\times \exp(-I^2 \sin^2\theta/4K_0^2)J_0(iI^2 \sin^2\theta/4K_0^2), \quad (2)$$

where J_0 is the zero-order Bessel function. One must now specify the form of $F(I)$ and integrate over I. Previously $F(I)$ has always been taken proportional to I up to some limiting value I_{max} and zero otherwise. Equation (2) must then be integrated numerically to yield an angular distribution which is characterized only by I_m and K_0. The I distribution is actually rounded rather than having a sharp cutoff, and for compound nuclei formed by charged particles with energies near the Coulomb barrier is approximately symmetric. The dependence of the anisotropy on the form of the I distribution has been investigated and some results are given in the Appendix. It turns out that since Eq. (2) is most sensitive to $\langle I^2 \rangle_{av}$, one can use the form $F(I) \propto I$ if one chooses $I_m^2 = 2\langle I^2 \rangle_{av}$. The dependence of $\langle I^2 \rangle_{av}$ on bombarding energy was determined from optical-model barrier transmission coefficients.[18]
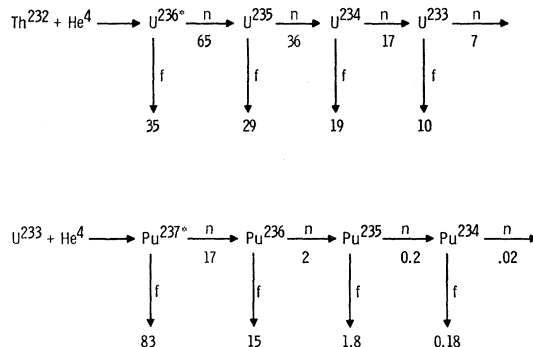

FIG. 4. Illustration of the relative probability for various members of the two decay chains formed by helium-ion-bombardment of U^{233} and Th^{232} to fission or to emit a neutron.

[15] R. Vandenbosch and J. R. Huizenga, *Proceedings of the Second United Nations Conference on the Peaceful Uses of Atomic Energy, Geneva, 1958* (United Nations, Geneva, 1958), Vol. 15, p. 284.
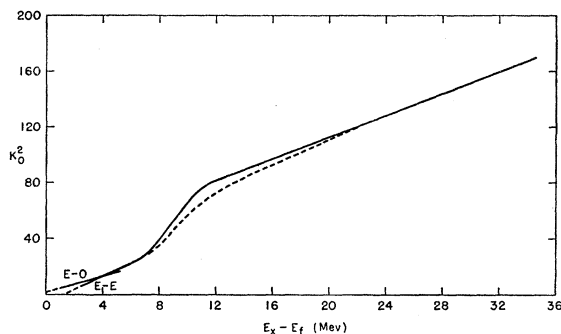
[16] J. E. Simmons and R. L. Henkel, Phys. Rev. **120**, 198 (1960).
[17] V. M. Strutinskii, *Proceedings of the International Conference on Nuclear Structure, Kingston, Canada, 1960* (University of Toronto Press, Toronto, 1960), p. 887.
[18] J. R. Huizenga and G. Igo, to be published. G. Igo, Phys. Rev. **115**, 1665 (1959).

Fig. 5. The dependence of $K_0{}^2$ on $E_x - E_f$. The lines for $E_x - E_f$ less than 6 Mev labeled E-O (even-odd) and E-E (even-even) have been taken from the analysis of Simmons and Henkel.[16] The solid curve and the dashed curve have been obtained from analysis of the energy dependence of the anisotropy for helium-ion-induced fission of U^{233}.

The angular distribution given by Eq. (2) when integrated over $F(I)$ is characterized only by $I_m{}^2$ and $K_0{}^2$. Since $I_m{}^2$ is known for each bombarding energy, the parameter to be determined from experiment is K_0 and its dependence on excitation energy. For the bombarding energies used in the present work, it is always energetically possible to have fission occurring both before and after neutron emission, complicating somewhat the deduction of $K_0{}^2$ as a function of excitation energy. However, fission induced by neutrons of 1–5 Mev can only take place before neutron emission, enabling a direct determination of $K_0{}^2$ at the lowest excitation energies. Extensive measurements of angular distributions for fission induced by neutrons have been reported,[16,19] and the dependence of $K_0{}^2$ on excitation energy as deduced by Simmons and Henkel[16] is shown in the lower left-hand corner of Fig. 5 for two nuclear types. The measure of the excitation energy is taken as the excitation energy in excess of the fission threshold, $E_x - E_f$. It is seen that the line for $K_0{}^2$ for even-odd compound nuclei extrapolates to the origin, whereas the line for even-even compound nuclei extrapolates to zero at approximately 1-Mev excitation energy. This is attributed to the fact that even-even nuclei have few levels below 1 Mev because of the pairing effect.

Now that the dependence of $K_0{}^2$ is known for lower excitation energies, it becomes easier to deduce $K_0{}^2$ at higher excitation energies from the experimental data reported in the present work. For a low alpha bombarding energy, the value of $K_0{}^2$ (and hence the anisotropy for fission following neutron emission) is known, and one can deduce $K_0{}^2$ at the higher excitation energy corresponding to fission prior to neutron emission. This process can be extended to the highest excitation energies reached in these experiments, $E_x - E_f \approx 35$ Mev. This analysis is most easily performed using the experimental data for the target U^{233}, as the percentage of fissions following neutron emission is the smallest for this case. The resulting determination of

[19] L. Blumberg and R. B. Leachman, Phys. Rev. 116, 102 (1959).

$K_0{}^2$ is shown as the solid line in Fig. 5. This functional dependence of $K_0{}^2$ deduced from the U^{233} data can now be used to predict the dependence on bombarding energy of the Th^{232} anisotropy. This calculation is shown (somewhat smoothed) as the solid line in Fig. 6. The fit to the U^{233} data is trivial, as it was used in deducing $K_0{}^2$. It should be remarked that in making these calculations one must know the energy carried away by the neutrons. This is not a fixed quantity, as the neutrons are emitted with a continuous spectrum of energies. This effect was approximated by dividing up the neutron spectrum into three parts, so that some averaging over residual excitation energy was accomplished. The neutron kinetic energy spectrum was obtained using a nuclear temperature given by $T = (E/10)^{\frac{1}{2}}$. In making these calculations published values of neutron binding energies[20] and fission thresholds[21] were used.

It was also assumed that $K_0{}^2$ is never less than 3, for as $K_0{}^2$ goes to zero the anisotropy tends toward infinity. The $K_0{}^2$ vs $E_x - E_f$ curves of Simmons and Henkel[16] extrapolate to $K_0{}^2 \cong 0$ at $E_x - E_f = 0$ for even-odd fissioning nuclei, and to $K_0{}^2 \cong 0$ at $E_x - E_f \cong 1$ Mev for even-even fissioning nuclei. However these extrapolated curves are not expected to hold in detail near threshold, as a statistical treatment is not valid at low excitation energies. The assumption that $K_0{}^2$ is never less than 3 cannot be important except for special cases, e.g., second-chance fission close to threshold. One would like to attribute the deviation between the calculated and experimental anisotropies below 23 Mev to an over-estimation of $I_m{}^2$ by the optical model used. However it is rather difficult to obtain the required change in $I_m{}^2$ by reasonable adjustment of the optical model parameters.

In the direction of $K_0{}^2$ described above it has been
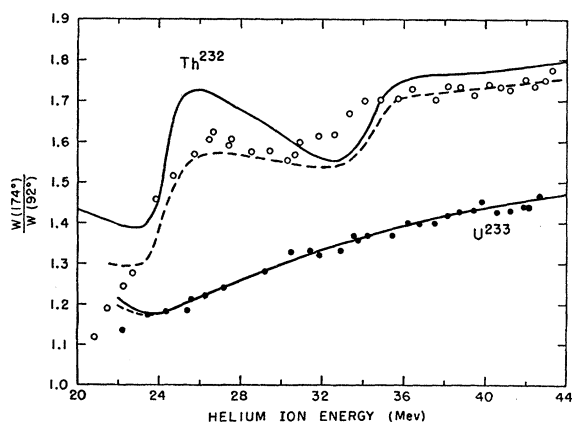

Fig. 6. Theoretical fits to the energy dependence of the anisotropy. The fit to the U^{233} data is not significant as it was used in deducing the parameter $K_0{}^2$. The solid curve and the dashed curve result from different assumptions in the analysis (see text).

[20] B. M. Foreman, Jr. and G. T. Seaborg, J. Inorg. and Nucl. Chem. 7, 305 (1958).
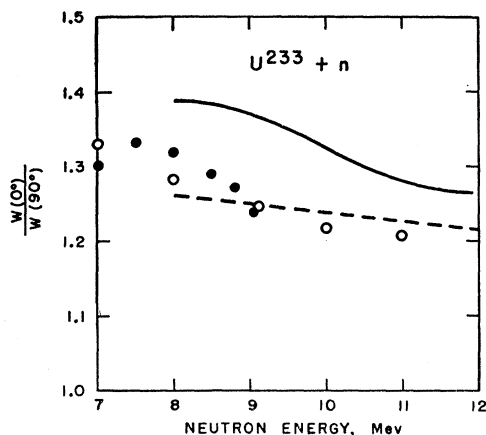[21] R. Vandenbosch and G. T. Seaborg, Phys. Rev. 110, 507 (1958).

FIG. 7. Angular anisotropy for neutron-induced fission of U[233]. The data represented by open circles are from reference 19 and the filled circles from reference 16. The solid and dashed curves represent theoretical calculations described in the text.

assumed that $I_m{}^2$ is not changed as a result of neutron emission. If, however, the spin distribution of the levels populated by neutron emission favors low spins, then there may be a reduction of $\langle I^2 \rangle_{av}$ and hence $I_m{}^2$ following neutron emission. Although there is not a great deal of detailed information known on the spin distribution of the level density and its dependence on excitation energy, recent experiments on isomer ratios[22,23] suggest that for excitation energies below 12 Mev the effective moment of inertia which determines the spin distribution is reduced to the point where one would expect $\langle I^2 \rangle_{av}$ to be reduced following neutron emission. There is evidence that this is taking place from angular distributions for fission induced by 8–11-Mev neutrons.[16,19] If one uses the branching ratios[15] for fission and neutron emission to find the proportion of second chance fission (fission following neutron emission) and calculates the anisotropy for this fraction of the fissions (from the $K_0{}^2$ values known from 1- to 5-Mev neutron-induced fission) one finds that all or even sometimes more than all of the anisotropy observed for 10-Mev neutrons must have come from the second chance fissions. Stating the problem another way, if you compute the anisotropy for 8- to 11-Mev neutron induced fission using the $K_0{}^2$ values given by the solid line in Fig. 5, the computed anisotropies are much too high, as is shown by the solid line in Fig. 7. These considerations suggest that the anisotropy of the second chance fissions has been overestimated, presumably because we have not taken into account the lowering of $\langle I^2 \rangle_{av}$ following neutron emission.

Since the parameters which would enable calculation of the reduction in $I_m{}^2$ following neutron emission are not known in detail, we have investigated what such a

reduction might do to calculated anisotropies by assuming a simple trial function. For residual excitation energies following neutron emission greater than 12 Mev, $I_m{}^2$ is assumed to be unchanged. For residual excitation energies E_R between 5 and 12 Mev the value of $I_m{}^{2\prime}$ following neutron emission is assumed to be $I_m{}^{2\prime} = 0.085\ E_R I_m{}^2$. Nuclei with excitation energy less than 5 Mev do not fission and need not be considered. The process of deducing $K_0{}^2$ from the anisotropy of helium-ion-induced fission of U[233] was repeated, giving rise to the broken curve in Fig. 5. The anisotropies for helium-ion-induced fission of Th[232] and for neutron-induced fission of U[233] were then recalculated using this new dependence of $K_0{}^2$ and the above-mentioned assumption about reduction of $I_m{}^2$, resulting in the broken curves in Figs. 6 and 7. The result is that the break in the curve for $K_0{}^2$ is somewhat smoothed out, the over-all fit to the Th[232] data is slightly improved, and the fit to the neutron-induced data is considerably better. Another refinement which might also be included is the dependence of fissionability on angular momentum. There are reasons to believe that compound nuclei with large angular momenta have a higher probability for fissioning compared to emitting a neutron than do nuclei with less angular momenta.[1,2] This effect would not only modify the I distribution $F(I)$ for the first chance fissions, but would tend to reduce $\langle I^2 \rangle_{av}$ for second and third chance fissions. For fission induced by heavy ions these effects are probably important, but it does not seem likely that they cause serious trouble in the present experiments. Since the parameters for calculating this effect are not well known this refinement has not been included in the calculations.

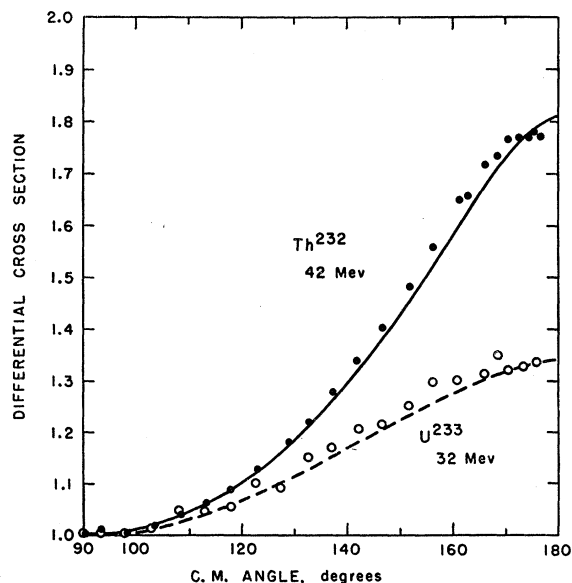As yet the theoretical calculations have been used

[22] J. R. Huizenga and R. Vandenbosch, Phys. Rev. 120, 1305 (1960).

[23] R. Vandenbosch and J. R. Huizenga, Phys. Rev. 120, 1313 (1960).

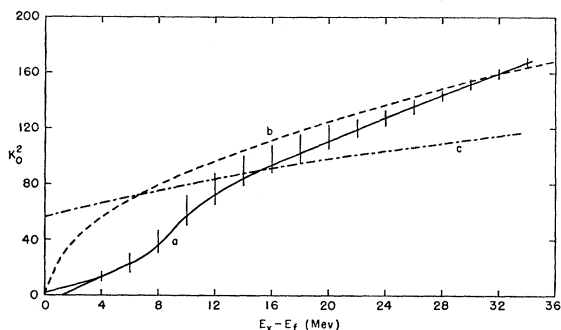FIG. 8. Comparison of experimental and calculated angular distributions for two representative cases.

FIG. 9. The solid line curve a is the dependence of K_0 vs $E_x - E_f$ as obtained from neutron-induced fission[16,19] and helium-ion-induced fission. The horizontal bars represent estimates of the uncertainty in this dependence. The dashed curve b is the prediction of the Halpern-Strutinskii, Griffin theory expected to be applicable at high excitation energies. The dash-dot-dash curve c illustrates the dependence predicted by the Ericson model (the ordinate represents $\sigma_1^2 + \sigma_2^2$ rather than K_0^2 in this case).

only to compare with the energy dependence of the anisotropy. Using the deduced dependence of K_0^2 on excitation energy (broken curve in Fig. 5) a detailed angular distribution can be calculated and compared with experiment. Such a comparison is shown in Fig. 8, where the fit to the data is shown to be quite satisfactory.

After consideration of the various uncertainties which arise in the derivation of K_0^2 as a function of excitation energy it is believed that the function must lie in the cross-hatched region of Fig. 9. It is seen that K_0^2 is best determined at the lowest and at the higher excitation energies, while unfortunately there is still some uncertainty in the intermediate region. It is interesting to compare these results with theoretical predictions for K_0^2. Using classical arguments[6] or statistical considerations[8] with a Fermi gas model it can be shown that

$$K_0{}^2 = \frac{T}{\hbar^2} \frac{\mathcal{I}_\perp \mathcal{I}_{\shortparallel}}{\mathcal{I}_\perp - \mathcal{I}_{\shortparallel}}, \tag{3}$$

where T is the nuclear temperature and $\mathcal{I}_\perp$ and $\mathcal{I}_{\shortparallel}$ are the moments of inertia of the nucleus at the saddlepoint perpendicular and parallel to the nuclear symmetry axis. If one estimates $\mathcal{I}_\perp \mathcal{I}_{\shortparallel}/(\mathcal{I}_\perp - \mathcal{I}_{\shortparallel})$ from the liquid drop calculations of Hiskes[24] using $r_0 = 1.2 \times 10^{-13}$ cm and assumes rigid rotation, one finds that the value of K_0^2 in Fig. 9 at 32 Mev corresponds to a nuclear temperature of about 1.6 Mev. From a Fermi gas model one expects the nuclear temperature to depend on the square root of the excitation energy, leading to a dependence for K_0^2 as indicated by the dashed line in Fig. 9. It is clear that for low excitation energies K_0^2 is much reduced, and it has been suggested[6,8] that this is a result of nuclear pairing effects. One knows that for even-even nuclei the pairing energy prevents intrinsic excitations with $K \neq 0$ for excitation energies less than

the approximately 1 Mev required to break a pair. If the cost in energy of breaking pairs persists beyond the first pair, one must expend excitation energy in breaking pairs that would otherwise be available for single-particle excitations. If after enough pairs are broken it no longer requires energy to break further pairs, one would expect K_0^2 to approach the Fermi gas dependence at the critical energy. Below the critical energy the pairing interactions are expected to reduce the values of K_0^2 from the Fermi gas model predictions. Indeed the derived values of K_0^2 are smaller than the Fermi gas model predictions at energies below 12 Mev. In addition the rise of K_0^2 in the 7- to 12-Mev region is less sharp than was suggested by an earlier analysis based on considerably scantier data, and hence is in better agreement with the expected slope of a superconductor model.

One of the basic assumptions in the Halpern-Strutinskii, Griffin theory of fission-fragment angular distributions is that the final K distribution is established at the saddle point. The K distribution is determined by the distribution of K values which characterizes intrinsic states of the nucleus at the saddle-point excitation energy. This model further postulates that the K distribution will not be altered at stages of the fission process beyond the saddle point.

In contrast to this model Ericson[25] has recently derived an expression for the fission fragment angular distribution by regarding fission as being entirely governed by the density of states after the process. In this treatment the saddle-point K values are not preserved and the angular distributions are determined by the sum of the parameters $(\sigma_1^2 + \sigma_2^2)$ which characterize the primary fission fragments, where σ_1^2 and σ_2^2 are the angular momentum cutoff factors in the spin-dependent level density expressions for the two fragments. Ericson[25] derives an expression for the angular distribution which is formally identical to that obtained by Halpern and Strutinskii, differing only in the replacement of the parameter K_0^2 by $\sigma_1^2 + \sigma_2^2$. Application of the Fermi gas model gives $\sigma_1^2 = T_1 \mathcal{I}_1/\hbar^2$ and $\sigma_2^2 = T_2 \mathcal{I}_2/\hbar^2$, where T and $\mathcal{I}$ are the nuclear temperature and moment of inertia of the residual nuclei. Since the excitation energy of each of the two fragments is approximately 10 Mev even for thermal fission $(E_x - E_f \simeq 0)$ this theory predicts a fairly large value of $(\sigma_1^2 + \sigma_2^2)$ at $E_x - E_f = 0$, and hence a smaller energy dependence of $(\sigma_1^2 + \sigma_2^2)$ compared to K_0^2 on $E_x - E_f$ at higher excitation energies. This dependence on $E_x - E_f$ is shown by the curve labeled c in Fig. 9 (remembering that K_0^2 now becomes $\sigma_1^2 + \sigma_2^2$). This curve has been constructed assuming rigid body moments of inertia and a level density parameter $(a = 10)$ which fits observed fission neutron kinetic energy distributions.[26] Another choice for the level density parameter could change the absolute value but not the excitation energy depend-

[24] J. R. Hiskes, University of California Radiation Laboratory Report UCRL-9275 (unpublished).

[25] T. Ericson, in *Advances in Physics*, edited by N. F. Mott (Taylor and Francis, Ltd., London, 1960), Vol. 9, p. 425.

[26] J. Terrell, Phys. Rev. **113**, 527 (1959).

TABLE II. Comparison of calculated anisotropies $(\sigma_{174°}/\sigma_{90°})$ for two forms of the distribution function $F(I)$. The entries in the second column were calculated using the distribution given by curve b in Fig. 10 and those in the third column using the distribution given by curve c. The anisotropies have been calculated for different values of the parameter K_0^2, listed in the first column.

K_0^2	$\sigma_{174°}/\sigma_{90°}$ (Distribution b)	$\sigma_{174°}/\sigma_{90°}$ (Distribution c)
2	5.1	5.2
4	3.72	3.8
8	2.63	2.72
16	1.92	1.94
40	1.41	1.40
80	1.21	1.18
160	1.10	1.08

ence. The failure of this model at low excitation energies was expected by Ericson. At higher excitation energies $(E_x - E_f > 20)$ the predicted dependence on excitation energy is considerably weaker than experimentally observed, suggesting that the K distribution is determined at the saddle point rather than at a later stage of the fission process. This supports the assumption of the earlier theoretical treatment that the passage from the saddle point to scission is fast enough that reorientations which would result in changes of K values do not occur appreciably.

ACKNOWLEDGMENTS

We are indebted to W. J. Ramler, M. C. Oselka, and the other members of the cyclotron group for their cooperation in performing these experiments. We are indebted to D. M. Sparlin, A. Jaffey, and E. Klema for the solid state detectors and suggestions concerning their use. We are grateful to W. Bentley for his assistance with the electronic equipment and to Miss M. Petheram for electroplating target material and reduction of data. We wish to thank A. Strecock, J. Scherer, and J. Bagby for programming for the computer problems connected with these experiments.

APPENDIX

The calculation of theoretical values of the angular distributions of fission fragments requires the integration of Eq. (2) over I, where $F(I)$ describes the distribu-
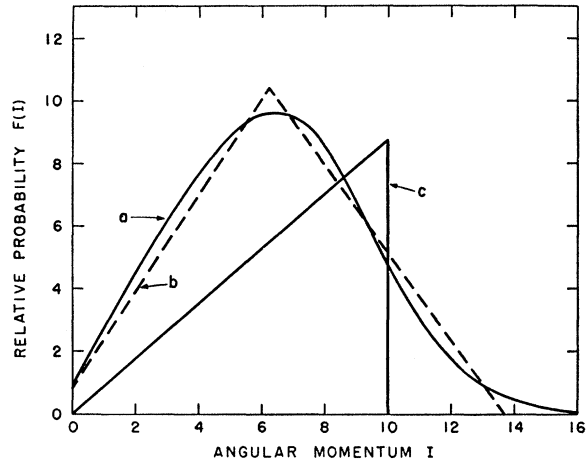

FIG. 10. Curve a shows the distribution in angular momentum I resulting from 26-Mev helium-ion bombardment of U^{233}. The triangular distribution b is an approximation to the true distribution a. Curve c is the sharp cutoff distribution which has the same value of $\langle I^2 \rangle_{av}$ as the true distribution a.

tion of angular momenta in the compound nucleus. A sharp cutoff approximation, where $F(I)$ is proportional to I up to some maximum value I_m, has usually been employed. If one computes $F(I) \approx (2l+1)T_l$ using optical model predictions for the barrier transmission coefficients T_l, one finds that $F(I)$ is quite rounded, especially for low bombarding energies. Curve a in Fig. 10 shows the distribution in I, $F(I)$, resulting from 26-Mev helium ion bombardment of U^{233}. We have approximated this distribution by the triangular distribution shown by curve b. Equation (2) was then integrated over the distribution given by curve b to yield calculated anisotropies as given in the second column of Table II. If instead one uses the linear approximation with a sharp cutoff one obtains anisotropies as given in column 3. The choice of I_m in the linear approximation shown by curve c was such that $\langle I^2 \rangle_{av}$ for distribution a and c were equal, making use of the fact that $2\langle I^2 \rangle_{av} = I_m^2$ for a linear distribution. It can be seen from comparison of columns 2 and 3 in Table II that the anisotropy is very nearly the same for the two distributions, so that for all the calculations described in the text we have used the linear approximation.